Supplementary Information for:

Surfactant Control of Interfacial Reaction Rates in Aqueous Microdroplets

Alexander M. Prophet,[1] David T. Limmer,[1,2,3,4] & Kevin R. Wilson[1*]

[1]*Chemical Sciences Division, Lawrence Berkeley National Laboratory, Berkeley, CA 94720*

[2]*Department of Chemistry, University of California, Berkeley, CA 94720*

[3]*Materials Science Division, Lawrence Berkeley National Laboratory, Berkeley, California 94720*

[4]*Kavli Energy NanoScience Institute, Berkeley, California 94720*

*Correspondence to krwilson@lbl.gov

Contents

SI-1: Experimental

SI-2: Model framework details

SI-3: Steady-state analysis

SI-4: Experimental data

SI-1: Experimental

Here we provide additional information about the experimental setup and reaction conditions. Fig. S1 provides a brief schematic of the experimental apparatus, indicating the major components of the electrodynamic balance and open-port sampling interface (OPSI). An example mass spectrum is provided in Fig. S2 showing the strong signal intensity at m/z = 126.9 resulting from the iodide ion. The citric acid (CA) buffer can also be observed both before and after the reaction.

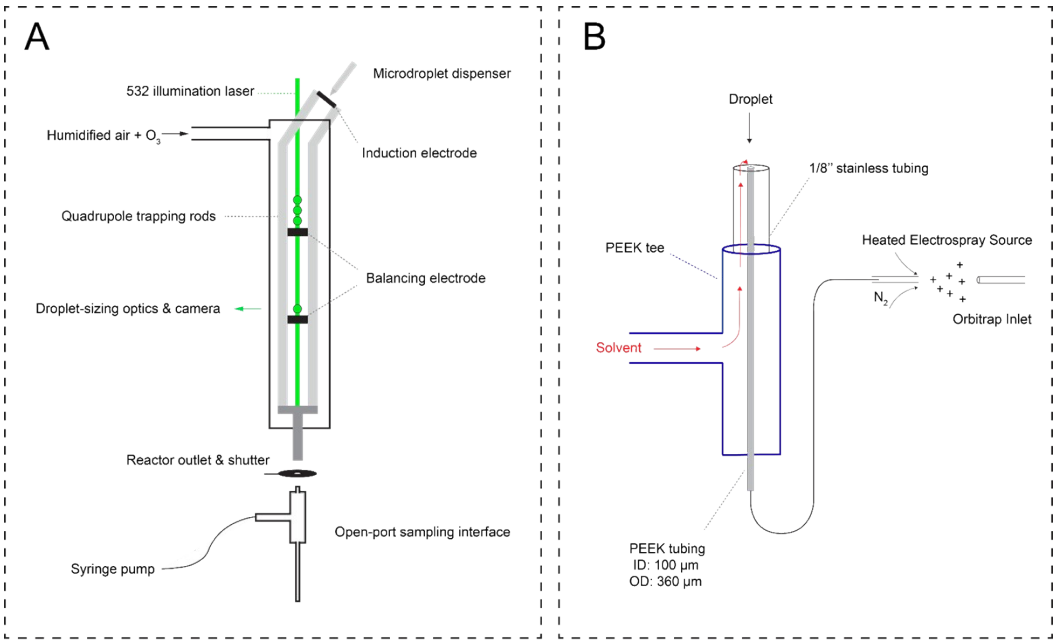

Fig. S1: Experimental diagram for (A) quadrupole electrodynamic trap (QET) with major components labeled and (B) open-port sampling interface (OPSI) for electrospray ionization mass spectrometry (ESI-MS).

An example of the Mie scattering phase function used to quantify the droplet radii for each experiment is shown in Fig. S3. The angular spacing between peaks in the interference pattern is used to identify the radius of a given microdroplet by referencing a library of simulated peak positions and spacings. The details of this approach and the algorithm employed can be found in previous work[1] and by Davies and co-workers.[2,3]

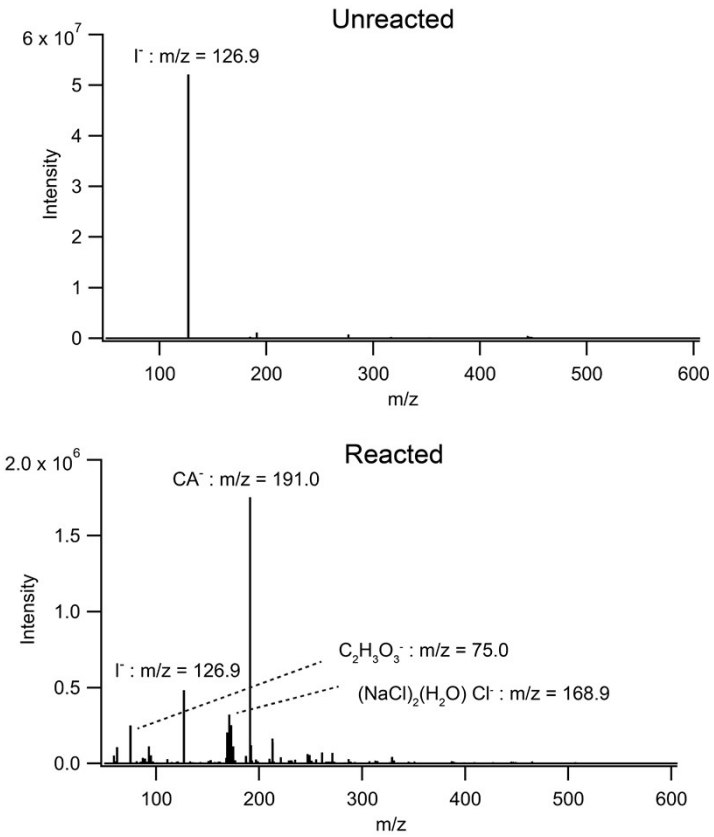

Fig. S2: Mass spectra for unreacted and reacted microdroplets containing NaI, NaCl, citric acid buffer at pH 3 with 32 µM of Triton X-100. The only noticeable change in the spectra is loss of I^- due to oxidation by O_3 and a more visible background.

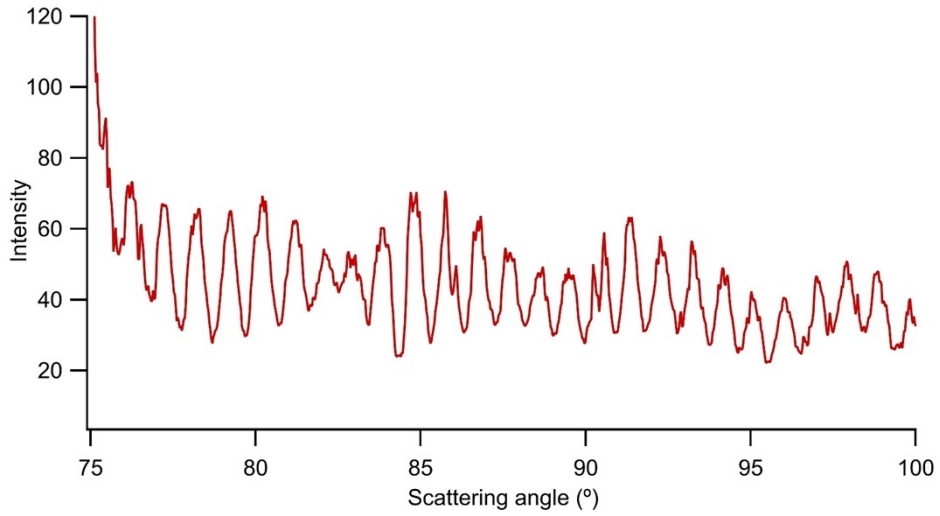

Fig. S3: Scattering intensity vs. collection angle for Mie scattering from a 17 µm radius droplet.

SI-2: Model Framework & Kinetic Simulations

The kinetic model used in the present analysis has been discussed extensively in recent publications.[4–6] For details on the conceptual model framework, we reference the reader to a previous work, which provides an overview of the updated framework to include sub-surface reactivity.[7] Each elementary reaction step used to generate the simulated kinetic profiles is also provided therein. The underlying chemical mechanism for this reaction system, including its pH dependence, was explored in more detail in previous work.[6] The current model framework follows exactly that described by Prophet *et al.*[7], reproduced here in Table S1, with addition of the Triton X-100 adsorption step as introduced in the main text, section IV. This additional adsorption step was included in the surface-compartment of the kinetic description to run all simulations.

Table S1: Elementary kinetic steps used to simulate the model in Kinetiscope©. Steps defined in the surface compartment are labeled S, diffusion coefficients for transfer between adjacent compartments are labeled D, steps defined in both the reaction-diffusion and inner-bulk compartment are labeled B, and the maximum coverage terms for each species are labeled G. As explored in the main text section IV, integers n = 3 and m = 5 are used to correct desolvation coefficients for TX and I^-, respectively, allowing TX and I^- to adsorb to the same set of surface sites (with maximum Γ_{∞}^{C}).

#	Step	Rate coefficient	Reference
S1	$O_{3(g)} \underset{k_{diff}}{\overset{k_{diff}}{\rightleftarrows}} O_{3(diff)}$	$k_{diff} = 1.06 \times 10^{9}\ s^{-1}$	7,8
S2	$O_{3(diff)} + site_{O_3} \underset{k_{des}}{\overset{k_{ads}}{\rightleftarrows}} O_{3(ads)}$	$k_{ads} = 1.77 \times 10^{-11}\ cm^3\ molec.^{-1} s^{-1}$ $k_{des} = 1.93 \times 10^{10}\ s^{-1}$	6
S3	$O_{3(ads)} \underset{k_{desolv}}{\overset{k_{solv}}{\rightleftarrows}} O_{3(b)} + site_{O_3}$	$k_{solv} = 1.9 \times 10^{8}\ s^{-1}$ $k_{desolv} = 1.2 \times 10^{-12}\ cm^3\ molec.^{-1} s^{-1}$	6
S4	$I_{(\bar{ads})} \underset{k_{desolv}}{\overset{k_{solv}}{\rightleftarrows}} I_{(\bar{blk})} + m\ site$	$k_{solv} = 10^{3}\ s^{-1}$ § $k_{desolv} = 1.66 \times 10^{-18}\ cm^3 \cdot molec.^{-1} \cdot s^{-1}$	9,10
S5	$IO_{(\bar{ads})} \underset{k_{desolv}}{\overset{k_{solv}}{\rightleftarrows}} IO_{(\bar{b})} + m\ site$	$k_{solv} = 1 \times 10^{3}\ s^{-1}$ § $k_{desolv} = 1.66 \times 10^{-18}\ cm^3 \cdot molec.^{-1} \cdot s^{-1}$	9,10
S6	$IO_{2(\bar{ads})} \underset{k_{desolv}}{\overset{k_{solv}}{\rightleftarrows}} IO_{2(\bar{b})} + m\ site$	$k_{solv} = 1 \times 10^{3}\ s^{-1}$ § $k_{desolv} = 1.66 \times 10^{-18}\ cm^3 \cdot molec.^{-1} \cdot s^{-1}$	9,10
S7	$TX_{(ads)} \underset{k_{desolv}}{\overset{k_{solv}}{\rightleftarrows}} TX_{(blk)} + n\ site$	$k_{solv} = 1\ s^{-1}$ †† $k_{desolv} = 1.1 \times 10^{-15}\ cm^3\ molec.^{-1} s^{-1}$	see section IV

S8	$I_{2(ads)} \underset{k_{desolv}}{\overset{k_{solv}}{\rightleftarrows}} I_{2(blk)} + m\,site$	$k_{solv} = 1 \times 10^{3}\ s^{-1}$ § $k_{desolv} = 1.66 \times 10^{-18}\ cm^{3} \cdot molec.^{-1} \cdot s^{-1}$	9,10
S9	$HOI_{(ads)} \underset{k_{desolv}}{\overset{k_{solv}}{\rightleftarrows}} HOI_{(blk)} + m\,site$	$k_{solv} = 1 \times 10^{3}\ s^{-1}$ § $k_{desolv} = 1.66 \times 10^{-18}\ cm^{3} \cdot molec.^{-1} \cdot s^{-1}$	9,10
S10	$I_{3(\bar{ads})} \underset{k_{desolv}}{\overset{k_{solv}}{\rightleftarrows}} I_{3(\bar{blk})} + m\,site$	$k_{solv} = 1 \times 10^{3}\ s^{-1}$ § $k_{desolv} = 1.66 \times 10^{-18}\ cm^{3} \cdot molec.^{-1} \cdot s^{-1}$	9,10
S11	$I_{(\bar{ads})} + O_{3(ads)} \overset{k_f}{\rightarrow} IO_{(\bar{ads})} + site_{O_3}$	$k_f = 1 \times 10^{-13}\ cm^{3} \cdot molec.^{-1} \cdot s^{-1}$	7
S12	$IO_{(\bar{ads})} + O_{3(ads)} \overset{k_f}{\rightarrow} IO_{2(\bar{ads})} + site_{O_3}$	$k_f = 1.66 \times 10^{-11}\ cm^{3} \cdot molec.^{-1} \cdot s^{-1}$	11
S13	$IO_{2(\bar{ads})} + O_{3(ads)} \overset{k_f}{\rightarrow} IO_{3(\bar{blk})} + m\,site + site_{O_3}$	$k_f = 1.66 \times 10^{-11}\ cm^{3} \cdot molec.^{-1} \cdot s^{-1}$	11
S14	$IO_{(\bar{ads})} + H^{+} \underset{k_r}{\overset{k_f}{\rightleftarrows}} HOI_{(ads)}$	$k_f = 1.66 \times 10^{-10}\ cm^{3} \cdot molec.^{-1} \cdot s^{-1}$ * $k_r = 1.58\ s^{-1}$	12,13
S15	$HOI_{(ads)} + I_{(\bar{ads})} \underset{k_r}{\overset{k_f}{\rightleftarrows}} I_2OH_{(\bar{ads})} + m\,site$	$k_f = 6.64 \times 10^{-17}\ cm^{3} \cdot molec.^{-1} \cdot s^{-1}$ $k_r = 1.34 \times 10^{2}\ s^{-1}$	14
S16	$I_2OH_{(\bar{ads})} + H^{+} \underset{k_r}{\overset{k_f}{\rightleftarrows}} I_{2(ads)}$	$k_f = 3.32 \times 10^{-11}\ cm^{3} \cdot molec.^{-1} \cdot s^{-1}$ * $k_r = 3.2\ s^{-1}$	14
S17	$HOI_{(ads)} + I_{(\bar{ads})} \underset{k_r}{\overset{k_f}{\rightleftarrows}} I_{2(ads)} + OH^{-} + m\,site$	$k_f = 3.5 \times 10^{-18}\ cm^{3} \cdot molec.^{-1} \cdot s^{-1}$ $k_r = 1.16 \times 10^{-16}\ cm^{3} \cdot molec.^{-1} \cdot s^{-1}$ *	15
S18	$HOI_{(ads)} + Cl^{-} + H^{+} \underset{k_r}{\overset{k_f}{\rightleftarrows}} ICl_{(ads)}$	$k_f = 8 \times 10^{-32}\ cm^{6}\ molec.^{-2}\ s^{-1}$ *‡ $k_r = 2.4 \times 10^{6}\ s^{-1}$	16
S19	$ICl_{(ads)} + Cl^{-} \underset{k_r}{\overset{k_f}{\rightleftarrows}} ICl_{2(\bar{ads})}$	$k_f = 1.66 \times 10^{-13}\ cm^{3}\ molec.^{-1}\ s^{-1}$ ‡ $k_r = 6 \times 10^{5}\ s^{-1}$	17
S20	$I_{2(ads)} + Cl^{-} \underset{k_r}{\overset{k_f}{\rightleftarrows}} I_2Cl_{(\bar{ads})}$	$k_f = 1.38 \times 10^{-16}\ cm^{3}\ molec.^{-1}\ s^{-1}$ ‡ $k_r = 5 \times 10^{4}\ s^{-1}$	17
S21	$I_{(\bar{ads})} + ICl_{(ads)} \underset{k_r}{\overset{k_f}{\rightleftarrows}} I_2Cl_{(\bar{ads})}$	$k_f = 1.83 \times 10^{-12}\ cm^{3}\ molec.^{-1}\ s^{-1}$ $k_r = 1.5\ s^{-1}$	17
S22	$I_{2(ads)} + I_{(\bar{ads})} \leftrightarrow I_{3(\bar{ads})} + m\,site$	$k_f = 1 \times 10^{-11}\ cm^{3} \cdot molec.^{-1} \cdot s^{-1}$ ¶ $k_r = 8.64 \times 10^{6}\ s^{-1}$	18

S23	$I_{2(ads)} \overset{k_{evap}}{\rightarrow} I_{2(g)} + m\ site$	$k_{evap} = 5.32 \times 10^{8}\ s^{-1}$ #	19
S24	$ICl_{(ads)} \overset{k_{evap}}{\rightarrow} ICl_{(g)} + m\ site$	$k_{evap} = 1.81 \times 10^{7}\ s^{-1}$ #	20
S25	$HOI_{(ads)} \overset{k_{evap}}{\rightarrow} HOI_{(g)} + m\ site$	$k_{evap} = 5.16 \times 10^{6}\ s^{-1}$ #	21
B1	$I_{(\bar{ads})} + O_{3(ads)} \overset{k_f}{\rightarrow} IO_{(\bar{ads})} + site_{O_3}$	$k_f = 2 \times 10^{-12}\ cm^3 \cdot molec.^{-1} \cdot s^{-1}$	22
B2	$IO_{(\bar{blk})} + O_{3(blk)} \overset{k_f}{\rightarrow} IO_{2(\bar{blk})}$	$k_f = 2.65 \times 10^{-15}\ cm^3 \cdot molec.^{-1} \cdot s^{-1}$	13
B3	$IO_{2(\bar{blk})} + O_{3(blk)} \overset{k_f}{\rightarrow} IO_{3(\bar{blk})}$	$k_f = 2.65 \times 10^{-15}\ cm^3 \cdot molec.^{-1} \cdot s^{-1}$	13
B4	$IO_{(\bar{blk})} + H^+ \underset{k_r}{\overset{k_f}{\rightleftarrows}} HOI_{(blk)}$	$k_f = 1.66 \times 10^{-10}\ cm^3 \cdot molec.^{-1} \cdot s^{-1}$ * $k_r = 1.58\ s^{-1}$	12,13
B5	$HOI_{(blk)} + I_{(\bar{blk})} \underset{k_r}{\overset{k_f}{\rightleftarrows}} I_2OH_{(\bar{blk})}$	$k_f = 6.64 \times 10^{-17}\ cm^3 \cdot molec.^{-1} \cdot s^{-1}$ $k_r = 1.34 \times 10^{2}\ s^{-1}$	14
B6	$I_2OH_{(\bar{blk})} + H^+ \underset{k_r}{\overset{k_f}{\rightleftarrows}} I_{2(blk)}$	$k_f = 3.32 \times 10^{-11}\ cm^3 \cdot molec.^{-1} \cdot s^{-1}$ * $k_r = 3.2\ s^{-1}$	14
B7	$HOI_{(blk)} + I_{(\bar{b})} \underset{k_r}{\overset{k_f}{\rightleftarrows}} I_{2(blk)} + OH^-$	$k_f = 3.5 \times 10^{-18}\ cm^3 \cdot molec.^{-1} \cdot s^{-1}$ $k_r = 1.16 \times 10^{-16}\ s^{-1}$ *	15
B8	$HOI_{(blk)} + Cl^- + H^+ \underset{k_r}{\overset{k_f}{\rightleftarrows}} ICl_{(blk)}$	$k_f = 8 \times 10^{-32}\ cm^6\ molec.^{-2}\ s^{-1}$ *‡ $k_r = 2.4 \times 10^{6}\ s^{-1}$	16
B9	$ICl_{(blk)} + Cl^- \underset{k_r}{\overset{k_f}{\rightleftarrows}} ICl_{2(\bar{blk})}$	$k_f = 1.66 \times 10^{-13}\ cm^3\ molec.^{-1}\ s^{-1}$ ‡ $k_r = 6 \times 10^{5}\ s^{-1}$	17
B10	$I_{2(blk)} + Cl^- \underset{k_r}{\overset{k_f}{\rightleftarrows}} I_2Cl_{(\bar{blk})}$	$k_f = 1.38 \times 10^{-16}\ cm^3\ molec.^{-1}\ s^{-1}$ ‡ $k_r = 5 \times 10^{4}\ s^{-1}$	17
B11	$I_{(\bar{blk})} + ICl_{(blk)} \underset{k_r}{\overset{k_f}{\rightleftarrows}} I_2Cl_{(\bar{blk})}$	$k_f = 1.83 \times 10^{-12}\ cm^3\ molec.^{-1}\ s^{-1}$ ‡ $k_r = 1.5\ s^{-1}$	17
B12	$I_{2(blk)} + I_{(\bar{blk})} \underset{k_r}{\overset{k_f}{\rightleftarrows}} I_{3(\bar{blk})}$	$k_f = 1 \times 10^{-11}\ cm^3 \cdot molec.^{-1} \cdot s^{-1}$ ¶ $k_r = 8.64 \times 10^{6}\ s^{-1}$	18
D1	$I_{(\bar{blk})}$	$D = 1.53 \times 10^{-5}\ cm^2 \cdot s^{-1}$ ¶	23
D2	$IO_{(\bar{blk})}$	$D = 1.53 \times 10^{-5}\ cm^2 \cdot s^{-1}$ †¶	23
D3	$IO_{2(\bar{blk})}$	$D = 1.53 \times 10^{-5}\ cm^2 \cdot s^{-1}$	23

		†¶	
D4	$IO_{3(blk)}^-$	$D = 1.53 \times 10^{-5}\ cm^2 \cdot s^{-1}$ †¶	23
D5	$I_2OH_{(blk)}^-$	$D = 1.53 \times 10^{-5}\ cm^2 \cdot s^{-1}$ †	23
D6	$I_2Cl_{(blk)}^-$	$D = 1.53 \times 10^{-5}\ cm^2 \cdot s^{-1}$ †	23
D7	$Cl_2I_{(blk)}^-$	$D = 1.53 \times 10^{-5}\ cm^2 \cdot s^{-1}$ †	23
D6	$I_{3(blk)}^-$	$D = 1.07 \times 10^{-5}\ cm^2 \cdot s^{-1}$	24
D7	$I_{2(blk)}$	$D = 1.15 \times 10^{-5}\ cm^2 \cdot s^{-1}$	25
D8	$HOI_{(blk)}$	$D = 1.15 \times 10^{-5}\ cm^2 \cdot s^{-1}$ †	25
D9	$ICl_{(blk)}$	$D = 1.15 \times 10^{-5}\ cm^2 \cdot s^{-1}$ †	25
D10	$O_{3(blk)}$	$D = 1.76 \times 10^{-5}\ cm^2 \cdot s^{-1}$	26
G1	O_3	$\Gamma_\infty^{O_3} = 5.42 \times 10^{14}\ molec.\ cm^{-2}$	27
G2	I^-	$\Gamma_\infty^{I^-} = 1.2 \times 10^{14}\ molec.\ cm^{-2}$	7
G3	TX	$\Gamma_\infty^{TX} = 2 \times 10^{14}\ molec.\ cm^{-2}$	see section IV
G4	All non-O_3 solutes	$\Gamma_\infty^{C} = 6 \times 10^{14}\ molec.\ cm^{-2}$	see section IV

§ Values of k_{desolv} found in these steps are divided by m = 5 in the Kinetiscope model to account for the larger maximum site value Γ_∞^C as explored in section IV.

†† The value of k_{desolv} found in the Triton X-100 adsorption step is divided by n = 3 in the Kinetiscope model to account for the larger maximum site value Γ_∞^C as explored in section IV.

* Simulated H^+ or OH^- are not explicitly included in the model, but rather, a pseudo-order rate condition is used by multiplying the reported rate coefficient with $[H^+]$ or $[OH^-]$ directly.

‡ As with the simulation of H^+, Cl^- is not included explicitly and initial $[Cl^-]$ for each experiment is used to calculate a pseudo-first order rate for each step involving Cl^-.

¶ These steps—either chemical or diffusional—involve a rapid equilibrium which can inhibit the stochastic simulation when run in concert. For many simulations, the corresponding constants shown in the table are decreased by ~100-1000 in order to allow for reasonable simulation times. However, we have verified that the model results have no observable sensitivity to these coefficients in the range we can observe.

† Diffusion coefficients for these species are estimated using the *D* for I^- for ions, and the *D* for I_2 for neutrals.

[#] Evaporation steps have also been defined in surface compartment as first order in the "bulk" species rather than adsorbed. This effectively allows I_2, for example, to evaporate from either the adsorbed or solvated state. While the model should technically only allow for adsorbed volatiles to evaporate, we define evaporation from the entire surface compartment to avoid potential coupling of evaporation rates with the solvation/desolvation rates of these volatiles, which we have largely treated as unknowns.

SI-3: Steady-state analysis methods

Here we provide further detail on the steady-state approach used to derive the analytical expressions. The core assumption used in this approach is that once the droplet is dispensed and the reaction has begun, a quasi-steady-state condition is quickly attained, which can be approximated by defining instantaneous concentrations of each species defined in the kinetic model framework. We briefly outline the derivation of the surfactant adsorption equations governing the "bulk-depletion" effect in microdroplets to demonstrate the utility of this approach and the origin of Eqs. 8-10a in section IV. Subsequently, we demonstrate how the same approach is used to quantify steady-state concentration of reactants [O_3] in the two relevant kinetic domains (*i.e.*, the surface and the subsurface "reaction-diffusion" region).

(i) Surfactant Adsorption

As illustrated in the main text, surfactant adsorption is treated as a set of elementary kinetic steps,

$$TX_{(blk)} + site \underset{k_{TX\_solv}}{\overset{k_{TX\_desolv}}{\rightleftarrows}} TX_{(ads)} \qquad \text{Step S1}$$

where the concentrations are described by a standard Langmuir-adsorption isotherm:

$$[TX_{(ads)}] = \frac{\Gamma_\infty^{TX} \; K_{eq}^{TX} \cdot [TX_{(blk)}]}{\delta \; 1 + K_{eq}^{TX} \cdot [TX_{(blk)}]} \qquad \text{Eq. S1}$$

Recall that $K_{eq}^{TX} = \frac{k_{TX\_desolv}}{k_{TX\_solv}}$ and that $\frac{\Gamma_\infty^{TX}}{\delta}$ represents the maximum concentration of available surface sites for Triton X-100. Because this derivation neglects the interfacial concentration of I^-, TX adsorption can be modeled as occupying a single site where Γ_∞^{TX} is used to define the maximum site number rather

than Γ_{∞}^{C} as discussed in section IV. The kinetics of surfactant adsorption in the microdroplet (Step S1) can be expressed as,

$$\frac{d[TX_{(ads)}]}{dt} = k_{TX\_desolv}\,[site][TX_{(blk)}] - k_{TX\_solv}[TX_{(ads)}] \qquad \text{Eq. S3}$$

We now use the steady-state assumption, $\frac{d[TX_{(ads)}]}{dt} = 0$, to relate the concentrations of $[TX_{(ads)}]$ and $[TX_{(blk)}]$,

$$k_{TX\_solv}[TX_{(ads)}] = k_{TX\_desolv}\,[site][TX_{(blk)}] \qquad \text{Eq. S4}$$

Where the available site concentration is,

$$[site] = \frac{\Gamma_{\infty}^{TX}}{\delta} - [TX_{(ads)}]. \qquad \text{Eq. S5}$$

Furthermore, $[TX_{(ads)}]$ and $[TX_{(blk)}]$ are related through the conservation of the total number of TX molecules present in the microdroplet, which provides the constraint,

$$[TX_{(blk)}]_0 = [TX_{(blk)}] + \frac{3\,\delta}{r}[TX_{(ads)}] \qquad \text{Eq. S6}$$

where δ is the thickness of the droplet interface (1 nm) and *r* is the droplet radius. In Eq. S6, $[TX_{(blk)}]_0$ is the bulk concentration at t = 0, where we assume $[TX_{(ads)}] = 0$. Solving Eqs. S4-S6 provides expressions for $[TX_{(ads)}]$ and $[TX_{(blk)}]$, presented in the main text as Eqs. 4 and 5. Lastly, we note that the approach outlined here assumes a static droplet radius *r*. Allowing *r* to change (due to evaporation or condensation of water, for example), provides similar equations, but with additional geometric factors.

(ii) Surface-Adsorbed and Solvated Ozone concentrations

An analogous approach is used to obtain expressions for ozone concentrations at the interface and within the sub-surface layer. While we do not provide an extensive discussion of how steady-state concentrations are derived, we provide a brief conceptual overview of the approach—while reserving a larger discussion to future work. The steady-state concentrations of O_3 at the interface and within the sub-surface are conceptually grounded in the kinetic model built in Kinetiscope. In the mechanics of this model, the surface adsorbed $O_{3(ads)}$ and the subsurface (or reaction-diffusion compartment) species $O_{3(rd)}$

are related through a solvation/desolvation process occurring in the top nm of solution, and a liquid diffusion description extending the length of the reaction-diffusion region. This is conceptually outlined in Fig. S4. As shown, this description invokes an intermediate "surface-to-bulk" species, termed $O_{3(sb)}$ that represents the O_3, which has undergone solvation across the interface but has yet to diffuse into the reaction-diffusion compartment. As such, no reaction for $O_{3(sb)}$ is defined as the species acts mostly as a bookkeeping concentration to define solvation and diffusion from the interface. In parallel, on the other side of the interface, a very similar approach is used to define another "gas-to-surface" species $O_{3(gs)}$, indicating ozone, which has diffused from the gas-phase to the droplet interface but has yet to undergo actual adsorption and thermal accommodation to the interface (or equivalently, O_3 which has desorbed from the interface, but has yet to diffuse away from the droplet surface). $O_{3(sb)}$ and $O_{3(gs)}$ are necessary to fully implement the steady state approach but are eliminated when solving for the species of interest $O_{3(ads)}$ and $O_{3(rd)}$. As noted in section IV, we choose to ignore the ozone reactivity in the inner bulk compartment, $[O_{3(blk)}]$ since the vast majority of reactivity occurs at the surface or in the reaction-diffusion region.

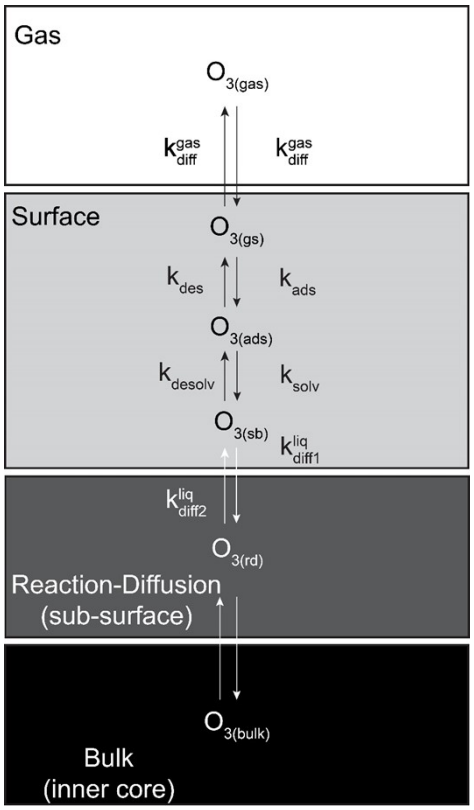

Fig. S4: Kinetic scheme showing mass transport pathways in model framework. The five related species can be used to create steady-state concentrations of $O_{3(ads)}$ and $O_{3(rd)}$ in the current work. As noted in the text, $O_{3(bulk)}$ is found to be negligible and so omitted in the analysis.

To solve for $[O_{3(ads)}]$ and $[O_{3(rd)}]$, rate equations are first defined for the four species identified, where $[O_{3(gas-\infty)}]$ represents the static gas phase concentration arbitrarily far from the droplet surface:

$$\frac{d[O_{3(gs)}]}{dt} = k_{diff}^{gas}[O_{3(gas)}] + k_{des}[O_{3(ads)}] - k_{diff}^{gas}[O_{3(gs)}] - \frac{\Gamma_{\infty(O_3)}}{\delta}k_{ads}\,[O_{3(gs)}] \quad \text{Eq. S7}$$

$$\frac{d[O_{3(ads)}]}{dt} = \frac{\Gamma_{\infty(O_3)}}{\delta}k_{ads}\,[O_{3(gs)}] + \frac{\Gamma_{\infty(O_3)}}{\delta}k_{desolv}[O_{3(sb)}] - k_{des}[O_{3(ads)}] - k_{solv}[O_{3(ads)}] - k_{rxn}^{srf}[I_{(\bar{ads})}][O_{3(ads)}]$$

Eq. S8

$$\frac{d[O_{3(sb)}]}{dt} = k_{solv}[O_{3(ads)}] + k_{diff1}^{liq}[O_{3(rd)}] - \frac{\Gamma_{\infty(O_3)}}{\delta}k_{desolv}\,[O_{3(sb)}] - k_{diff1}^{liq}[O_{3(sb)}] \quad \text{Eq. S9}$$

$$\frac{d[O_{3(rd)}]}{dt} = k_{diff2}^{liq}[O_{3(sb)}] - k_{diff2}^{liq}[O_{3(rd)}] - k_{rxn}^{blk}[I_{(\bar{rd})}][O_{3(rd)}] \quad \text{Eq. S10}$$

Kinetic coefficients found in Eq. S7-S10 can be found in the associated kinetic simulation description. The liquid diffusion rate coefficients k_{diff}^{liq1} and k_{diff}^{liq2} have not been defined in the previous work, but are simply defined through the application of Fick's first law,

$$k_{diff1}^{liq} = \frac{2D}{(L_{RD} + \delta)\delta}$$

$$k_{diff2}^{liq} = \frac{2D}{(L_{RD} + \delta)L_{RD}}$$

where L_{rxn} is the reaction diffusion length of O_3 in solution given the initial $[I^-]$, (which also defines the length of the RD compartment).

Applying a steady-state assumption, all differentials Eq. S7-S10 are assumed to be zero, enabling one to solve for each of the four concentrations in terms of the overall gas concentration $[O_{3(gas)}]$ and the iodide concentration, (where $[I_{(\bar{rd})}]$ and $[I_{(\bar{ads})}]$) are related through a Langmuir isotherm as outlined in the

main text. Solving in this manner produces expressions for $[O_{3(ads)}]$ and $[O_{3(rd)}]$ as given in Eq. 11 and Eq. 12 in the main text.

SI-4: Experimental data

Tables S2 and S3 below contain the data found in the main text Fig. 3 and Fig. 4, respectively.

Table S2: Remaining iodide fraction [I]/[I0] vs. time for the 9 [Triton X-100] conditions shown in Figure 3.

[TX] = 3.2 mM

t(s)	[I]/[I0]
0	1
90.36041	0.972053
91.49917	0.899438
92.00317	0.872377
180.2768	0.922999
181.5986	0.828855
183.9115	0.817199
271.9432	0.773728
272.355	0.753597
273.4548	0.863109
360.0527	0.740351
360.2116	0.780914
361.5614	0.765594
451.539	0.661134
452.4257	0.721418
457.5618	0.696534
539.8215	0.799057
541.063	0.631975
542.9855	0.675093
633.7419	0.704659
633.8693	0.629868
643.3516	0.614147
723.0465	0.493621
725.1078	0.630106
776.2303	0.465749
809.8386	0.610455
814.5882	0.404689
871.6723	0.468558
901.665	0.550426
905.3548	0.36423
955.2658	0.401825
993.6517	0.453267
1035.28	0.311521
1042.395	0.329933
1080.24	0.438545
1112.144	0.256738
1171.14	0.420848
1261.089	0.384586

[TX] = 1.6 mM

t(s)	[I]/[I0]
0	1
68.60367	0.941108
91.87155	0.933417
161.8164	0.925311
162.2201	0.901734
182.0457	0.849768
252.8746	0.902986
276.4327	0.836434
278.9972	0.74914
341.7416	0.874727
359.7966	0.762889
361.3009	0.799444
429.3405	0.812103
447.53	0.736387
461.2344	0.695196
524.0389	0.656049
538.0863	0.659208
541.1395	0.674262
610.2761	0.634606
625.4366	0.649227
630.3615	0.637886
702.2406	0.624691
714.5723	0.600461
723.2701	0.534502
790.2938	0.582197
816.9949	0.426392
834.2558	0.506673
881.1767	0.489662
899.6164	0.474819
979.9073	0.479508
989.0462	0.368439
1061.559	0.413941
1078.317	0.319998
1165.632	0.300649

[TX] = 795 µM

t(s)	[I]/[I0]
0	1
94.29367	0.943313
100.418	0.964155
117.6859	0.915194
181.2616	0.899957
203.1313	0.892552
206.5912	0.932396
269.311	0.829525
284.671	0.829321
294.5551	0.893031
370.1999	0.840027
379.4746	0.686441
388.0181	0.771322
460.4424	0.730769
468.9614	0.594975
474.2812	0.76145
550.044	0.680043
554.5338	0.661559
569.4648	0.700266
642.9516	0.649709
646.661	0.606163
655.8139	0.693108
731.7766	0.607016
738.2686	0.594143
744.0001	0.614738
822.8745	0.439042
833.0949	0.593173
836.2871	0.494198
923.3287	0.403795
923.7123	0.313782
924.8827	0.490657
1002.768	0.280267
1014.197	0.433962
1016.068	0.371003
1099.097	0.217132
1108.174	0.294165
1180.427	0.230549
1186.182	0.215913
1190.362	0.310158
1279.029	0.135969
1285.178	0.274864
1292.997	0.258373
1402.529	0.192369
1438.198	0.145476
1495.386	0.106903
1565.89	0.112603

[TX] = 480 μM

t(s)	[I]/[I0]
0	1
84.69891	0.942126
88.46592	0.957325
104.3051	0.952368
172.0875	0.890933
179.2902	0.912095
193.1422	0.904611
268.4698	0.79633
283.9406	0.795035
286.39	0.865337
358.5783	0.74533
377.369	0.75913
386.1213	0.673887
449.0538	0.712881
466.4496	0.734347
472.074	0.746857
537.4401	0.558204
549.6645	0.738501
564.5766	0.52448
627.0767	0.540835
647.9009	0.554333
674.394	0.539036
719.6438	0.401638
735.8426	0.557874
786.4938	0.529982
824.94	0.461542
879.8166	0.423068
931.6089	0.409995
1026.396	0.319377
1129.791	0.296788
1219.285	0.141129
1326.382	0.201688
1416.13	0.186981

[TX] = 320 μM

t(s)	[I]/[I0]
0	1
63.27279	0.929419
74.73716	0.832809
75.34892	0.867284
79.35129	0.834247
88.61755	0.898669
152.3515	0.784934
154.3175	0.636998
155.8921	0.795828
159.7847	0.711462
179.4089	0.784911
230.2467	0.540799
233.6644	0.69982
233.814	0.655915
247.6168	0.703501
268.4765	0.627282
301.9635	0.541274
309.0907	0.602519
311.7306	0.52393
334.1739	0.611554
359.4927	0.541619
383.7213	0.468159
385.6816	0.370835
395.9027	0.406359
430.0726	0.472355
447.9742	0.392043
461.9475	0.29808
462.285	0.31389
468.3296	0.3078
517.765	0.426404
535.9505	0.273737
538.3924	0.340694
603.7854	0.269392
614.9093	0.193318
627.8123	0.26315
683.1727	0.104275
694.1448	0.237401
718.0181	0.090287
783.2732	0.153139

[TX] = 160 μM

t(s)	[I]/[I0]
0	1
16.98968	0.972285
70.0993	0.887987
103.9617	0.860194
154.5488	0.802265
159.2003	0.771595
219.9647	0.589775
246.1819	0.580405
255.2953	0.610692
310.4597	0.344354
334.3647	0.376014
341.3823	0.423031
384.3336	0.241218
425.0009	0.164256
425.7025	0.260175
477.9844	0.07881
507.7503	0.065203
516.784	0.111471
605.5523	0.024869

[TX] = 64 µM

t(s)	[I]/[I0]
0	1
63.51167	0.878363
65.60404	0.931542
66.67746	0.934786
89.52655	0.774935
151.4541	0.6674
151.619	0.725185
155.1347	0.728459
185.8525	0.486738
242.6117	0.482232
246.9751	0.460082
247.48	0.434373
270.7734	0.28479
334.9728	0.301194
336.5328	0.233271
340.9347	0.294633
366.7276	0.105533
424.3504	0.095543
425.6941	0.107537
432.6504	0.08602
450.8464	0.038953
511.306	0.039346
522.7744	0.025746

[TX] = 32 µM

t(s)	[I]/[I0]
0	1
19.23641	0.963451
27.14305	0.943681
75.37341	0.819437
75.87229	0.779135
96.42572	0.78981
118.138	0.74866
148.9261	0.672176
155.4217	0.56953
174.096	0.670361
208.6014	0.439933
222.2936	0.584967
233.9087	0.429919
259.3312	0.453048
297.9865	0.342982
299.1205	0.409948
309.395	0.304532
375.8073	0.191398
389.2492	0.120193
390.887	0.155641
447.1145	0.11648
474.8565	0.088448
525.7865	0.056933
618.3368	0.014785

[TX] = 6 µM

t(s)	[I]/[I0]
0	1
54.18542	0.919309
66.70231	0.894943
105.588	0.779931
143.8691	0.773078
160.8622	0.59645
195.247	0.620364
232.0792	0.586559
248.266	0.521944
298.6154	0.462556
326.2488	0.386493
344.7067	0.372628
388.8573	0.30658
411.2404	0.230212
456.0869	0.139764
484.5432	0.156118
507.9547	0.079761
573.1509	0.062965
598.6583	0.032752

Table S3: Experimental uptake coefficients vs [Triton X-100] as shown in Figure 4.

[TX] (mM)	Uptake
0.0064	5.42E-03
0.0064	5.48E-03
0.0064	5.68E-03
0.0318	5.72E-03
0.0318	5.42E-03
0.0318	5.19E-03
0.0636	5.60E-03
0.0636	5.56E-03
0.0636	5.56E-03
0.0636	5.57E-03
0.0636	5.71E-03
0.0636	5.64E-03
0.1590	4.40E-03
0.1590	4.76E-03
0.1590	4.84E-03
0.3180	3.77E-03
0.3180	3.45E-03
0.3180	3.90E-03
0.3180	3.31E-03
0.3180	3.53E-03

[TX] (mM)	Uptake
0.4771	2.37E-03
0.4771	1.89E-03
0.4771	1.71E-03
0.4771	1.93E-03
0.6361	1.38E-03
0.6361	1.42E-03
0.6361	1.43E-03
0.7951	1.40E-03
0.7951	1.60E-03
0.7951	1.73E-03
1.5902	1.59E-03
1.5902	1.69E-03
1.5902	1.45E-03
3.1803	1.50E-03
3.1803	1.68E-03
3.1803	1.37E-03

Supplementary Reference:

(1) Willis, M. D.; Rovelli, G.; Wilson, K. R. Combining Mass Spectrometry of Picoliter Samples with a Multicompartment Electrodynamic Trap for Probing the Chemistry of Droplet Arrays. *Anal. Chem.* **2020**, *92* (17), 11943–11952. https://doi.org/10.1021/acs.analchem.0c02343.

(2) Davies, J. F. Mass, Charge, and Radius of Droplets in a Linear Quadrupole Electrodynamic Balance. *Aerosol Sci. Technol.* **2019**, *53* (3), 309–320. https://doi.org/10.1080/02786826.2018.1559921.

(3) Kaur Kohli, R.; Davis, R. D.; Davies, J. F. Tutorial: Electrodynamic Balance Methods for Single Particle Levitation and the Physicochemical Analysis of Aerosol. *J. Aerosol Sci.* **2023**, *174*, 106255. https://doi.org/10.1016/j.jaerosci.2023.106255.

(4) Willis, M. D.; Wilson, K. R. Coupled Interfacial and Bulk Kinetics Govern the Timescales of Multiphase Ozonolysis Reactions. *J. Phys. Chem. A* **2022**, *126* (30), 4991–5010. https://doi.org/10.1021/acs.jpca.2c03059.

(5) Wilson, K. R.; Prophet, A. M.; Willis, M. D. A Kinetic Model for Predicting Trace Gas Uptake and Reaction. *J. Phys. Chem. A* **2022**, *126* (40), 7291–7308. https://doi.org/10.1021/acs.jpca.2c03559.

(6) Prophet, A. M.; Polley, K.; Van Berkel, G. J.; Limmer, D. T.; Wilson, K. R. Iodide Oxidation by Ozone at the Surface of Aqueous Microdroplets. *Chem. Sci.* **2024**, *15* (2), 736–756. https://doi.org/10.1039/D3SC04254E.

(7) Prophet, A. M.; Polley, K.; Brown, E. K.; Limmer, D. T.; Wilson, K. R. Distinguishing Surface and Bulk Reactivity: Concentration-Dependent Kinetics of Iodide Oxidation by Ozone in Microdroplets. *J. Phys. Chem. A* **2024**, *128* (41), 8970–8982. https://doi.org/10.1021/acs.jpca.4c05129.

(8) Prophet, A.; Wilson, K. A Compartmentalized Model of Multiphase Chemical Kinetics. ChemRxiv February 20, 2025. https://doi.org/10.26434/chemrxiv-2025-9dw51.

(9) Jungwirth, P.; Tobias, D. J. Ions at the Air/Water Interface. *J. Phys. Chem. B* **2002**, *106* (25), 6361–6373. https://doi.org/10.1021/jp020242g.

(10) Woods, E.; Konys, C. A.; Rossi, S. R. Photoemission of Iodide from Aqueous Aerosol Particle Surfaces. *J. Phys. Chem. A* **2019**, *123* (13), 2901–2907. https://doi.org/10.1021/acs.jpca.8b12323.

(11) Bhujel, M.; L. Marshall, D.; T. Maccarone, A.; I. McKinnon, B.; J. Trevitt, A.; Silva, G. da; J. Blanksby, S.; J. Poad, B. L. Gas Phase Reactions of Iodide and Bromide Anions with Ozone: Evidence for Stepwise and Reversible Reactions. *Phys. Chem. Chem. Phys.* **2020**, *22* (18), 9982–9989. https://doi.org/10.1039/D0CP01498B.

(12) Paquette, J.; Wren, J. C.; Sunder, S.; Ford, B. L. *The Disproportionation of Iodine (I)*; 0-7058-1073–9; United Kingdom, 1986; pp 29–45.

(13) Bichsel, Y.; von Gunten, U. Oxidation of Iodide and Hypoiodous Acid in the Disinfection of Natural Waters. *Environ. Sci. Technol.* **1999**, *33* (22), 4040–4045. https://doi.org/10.1021/es990336c.

(14) Lengyel, I.; Epstein, I. R.; Kustin, K. Kinetics of Iodine Hydrolysis. *Inorg. Chem.* **1993**, *32* (25), 5880–5882. https://doi.org/10.1021/ic00077a036.

(15) Sebők-Nagy, K.; Körtvélyesi, T. Kinetics and Mechanism of the Hydrolytic Disproportionation of Iodine. *Int. J. Chem. Kinet.* **2004**, *36* (11), 596–602. https://doi.org/10.1002/kin.20033.

(16) Wang, Y. L.; Nagy, J. C.; Margerum, D. W. Kinetics of Hydrolysis of Iodine Monochloride Measured by the Pulsed-Accelerated-Flow Method. *J. Am. Chem. Soc.* **1989**, *111* (20), 7838–7844. https://doi.org/10.1021/ja00202a026.
(17) Margerum, D. W.; Dickson, P. N.; Nagy, J. C.; Kumar, K.; Bowers, C. P.; Fogelman, K. D. Kinetics of the Iodine Monochloride Reaction with Iodide Measured by the Pulsed-Accelerated-Flow Method. *Inorg. Chem.* **1986**, *25* (27), 4900–4904. https://doi.org/10.1021/ic00247a025.
(18) Palmer, D. A.; Ramette, R. W.; Mesmer, R. E. Triiodide Ion Formation Equilibrium and Activity Coefficients in Aqueous Solution. *J. Solut. Chem.* **1984**, *13* (9), 673–683. https://doi.org/10.1007/BF00650374.
(19) Sanemasa, I.; Kobayashi, T.; Piao, C. Y.; Deguchi, T. Equilibrium Solubilities of Iodine Vapor in Water. *Bull. Chem. Soc. Jpn.* **1984**, *57* (5), 1352–1357. https://doi.org/10.1246/bcsj.57.1352.
(20) Sander, R. Compilation of Henry's Law Constants (Version 5.0.0) for Water as Solvent. *Atmospheric Chem. Phys.* **2023**, *23* (19), 10901–12440. https://doi.org/10.5194/acp-23-10901-2023.
(21) Lin, C.-C. Volatility of Iodine in Dilute Aqueous Solutions. *J. Inorg. Nucl. Chem.* **1981**, *43* (12), 3229–3238. https://doi.org/10.1016/0022-1902(81)80094-2.
(22) Liu, Q.; Schurter, L. M.; Muller, C. E.; Aloisio, S.; Francisco, J. S.; Margerum, D. W. Kinetics and Mechanisms of Aqueous Ozone Reactions with Bromide, Sulfite, Hydrogen Sulfite, Iodide, and Nitrite Ions. *Inorg. Chem.* **2001**, *40* (17), 4436–4442. https://doi.org/10.1021/ic000919j.
(23) Dunlop, P. J.; Stokes, R. H. The Diffusion Coefficients of Sodium and Potassium Iodides in Aqueous Solution at 25°1. *J. Am. Chem. Soc.* **1951**, *73* (11), 5456–5457. https://doi.org/10.1021/ja01155a520.
(24) Darrall, K. G.; Oldham, G. The Diffusion Coefficients of the Tri-Iodide Ion in Aqueous Solutions. *J. Chem. Soc. Inorg. Phys. Theor.* **1968**, 2584. https://doi.org/10.1039/j19680002584.
(25) Gregory, D. P.; Riddiford, A. C. 731. Transport to the Surface of a Rotating Disc. *J. Chem. Soc. Resumed* **1956**, 3756. https://doi.org/10.1039/jr9560003756.
(26) Gottschalk, C.; Libra, J. A.; Saupe, A. *Ozonation of Water and Waste Water: A Practical Guide to Understanding Ozone and Its Applications*, 2nd Edition.; Wiley-VCH Verlag GmbH & Co., 2010.
(27) Vieceli, J.; Roeselová, M.; Potter, N.; Dang, L. X.; Garrett, B. C.; Tobias, D. J. Molecular Dynamics Simulations of Atmospheric Oxidants at the Air−Water Interface: Solvation and Accommodation of OH and O3. *J. Phys. Chem. B* **2005**, *109* (33), 15876–15892. https://doi.org/10.1021/jp051361+.